

# Preparation and characterization of a magnetically separated photocatalyst and its catalytic properties

Yuan Gao, Baohua Chen, Hulin Li, Yongxiang Ma\*

*Department of Chemistry, Lanzhou University, Lanzhou 730000, PR China*

Received 5 June 2002; received in revised form 15 October 2002; accepted 29 October 2002

## Abstract

A kind of loaded photocatalyst of  $\text{TiO}_2/\gamma\text{-Fe}_2\text{O}_3$  (TF) that can photodegrade organic pollutants in the dispersion system effectively and can be recycled easily by a magnetic field is reported in this paper. The structural features of TF catalyst sintered at different temperatures (in the range 200–900 °C) have been investigated by X-ray diffraction, atomic force microscope and transmission electron microscope studies. Phase composition and crystallinity change with the increasing sintering temperature of the specimens. The TF photocatalyst is composed of two parts: (1)  $\text{TiO}_2$  shell used for photocatalysis; (2)  $\gamma\text{-Fe}_2\text{O}_3$  core for separation by the magnetic field. Due to the strong light absorption by  $\gamma\text{-Fe}_2\text{O}_3$ , when the amount of the loaded  $\text{TiO}_2$  content was under 30% in the catalyst, the photocatalytic activity of TF was significantly lower than that of the pure  $\text{TiO}_2$ . On the other hand, the photocatalytic activity of TF reduced to a large extent at high sintering temperature (900 °C) owing to the presence of inactive ( $\text{Fe}_2\text{TiO}_5$ ) pseudobrookite phase. The sample sintered at 500 °C showed the highest activity for the degradation of aqueous solution of acridine dye.

© 2002 Elsevier Science B.V. All rights reserved.

**Keywords:** Photocatalyst;  $\gamma\text{-Fe}_2\text{O}_3$ ; Acridine dye

## 1. Introduction

In recent years, the heterogeneous photocatalysis for total oxidation of organic and inorganic water pollutants has been studied extensively [1,2]. Environmental purification using  $\text{TiO}_2$  photocatalysts has attracted a great deal of attention with the increasing number of recent environmental problems in the world [3–6]. Irradiating pulverulent semi-conductors like  $\text{TiO}_2$  in suspension, in aqueous solutions containing organic pollutants, creates a redox environment able to destroy these pollutants [7,8]. But photocatalysts are often applied as suspensions, costly problems associated with catalyst leaching, settling, floatation and the need for eventual catalyst separation by filtration during post-treatment, hinder their wide scale application in industry. Therefore, catalyst immobilization related research has attracted wide attention [9]. Simple coating [10–13] of the catalyst over glass, zeolite, silica, and ceramic, however, the activity of  $\text{TiO}_2$  photocatalyst in the fixed bed system is reduced to a considerable extent because the effective surface area of photocatalyst decreases considerably after the immobility of titania. In the dispersion system, Modestov et al.

[14] reported a kind of porous methyl silicate floating titania composites, which works at the gas–liquid intersurface, and is quite good for purification of oil slick and floating pollutants, but not pertinent for dealing with the soluble pollutants in the solution. Recently, Chen and Zhao [15] reported a kind of magnetically separable photocatalyst of  $\text{TiO}_2/\text{SiO}_2/\gamma\text{-Fe}_2\text{O}_3$  prepared by the solid phase synthesis method, which could be separated easily from the solution by a magnetic field and had a good photocatalytic activity. Addition of a  $\text{SiO}_2$  membrane between the  $\gamma\text{-Fe}_2\text{O}_3$  core and the  $\text{TiO}_2$  shell weakens the adverse influence of  $\gamma\text{-Fe}_2\text{O}_3$  on the photocatalysis of  $\text{TiO}_2$ . However, the detailed characterization researches of magnetically separated photocatalyst have not been done yet. The catalytic activity of  $\text{TiO}_2/\gamma\text{-Fe}_2\text{O}_3$  largely depends on preparation methods, titania content, sintering temperature and phase composition. In the present article, the magnetically separated photocatalyst of  $\text{TiO}_2/\gamma\text{-Fe}_2\text{O}_3$  was prepared by the finer  $\text{Fe}_3\text{O}_4$  powder dispersed in the  $\text{TiO}_2$  sol, forming  $\text{TiO}_2/\text{Fe}_3\text{O}_4$  granulated gel in the supersonic oscillator and then sintered at 500 °C for about 5 h. Compared with the solid phase synthesis method [15], the  $\text{TiO}_2$  shell prepared by the sol–gel method is able to enwrap the  $\text{Fe}_2\text{O}_3$  magnetic core effectively and reduce the strong light absorption of  $\gamma\text{-Fe}_2\text{O}_3$  particles under light irradiation. As  $\text{Fe}_3\text{O}_4$

\* Corresponding author.

E-mail address: [liuht@lzu.edu.cn](mailto:liuht@lzu.edu.cn) (Y. Ma).

crystallinity sintered above 200 °C can transform into  $\gamma$ -Fe<sub>2</sub>O<sub>3</sub>, the TiO<sub>2</sub>/ $\gamma$ -Fe<sub>2</sub>O<sub>3</sub> magnetically separated photocatalyst was obtained through sintering TiO<sub>2</sub>/Fe<sub>3</sub>O<sub>4</sub> granulated gel and the preparation process of Fe<sub>3</sub>O<sub>4</sub> nanoparticle is relatively simpler than that of  $\gamma$ -Fe<sub>2</sub>O<sub>3</sub>. The present work was also undertaken in an attempt to correlate the photocatalytic property of TiO<sub>2</sub>/ $\gamma$ -Fe<sub>2</sub>O<sub>3</sub> with titania content, phase composition, sintering temperature and reaction condition. The photocatalytic activities of TiO<sub>2</sub>/ $\gamma$ -Fe<sub>2</sub>O<sub>3</sub> photocatalyst was measured using an acridine dye solution as a model.

## 2. Experimental

Magnetic material of Fe<sub>3</sub>O<sub>4</sub> particles was prepared by aging ferrous hydroxide gels under simple experimental conditions without dustproof equipment [16]. Oxygen-free ferrous sulfate and potassium nitrate solutions were added slowly into an oxygen-free potassium hydroxide solution respectively under vigorous stirring for 30 min. After addition, the vessel containing 500 ml ferrous hydroxide gels was plugged and kept at 90 °C for 5 h to form Fe<sub>3</sub>O<sub>4</sub> deposits. Then the deposit was well washed with water, 1 mol l<sup>-1</sup> nitric acid and water, and was separated by magnetic levitation, this process was repeated several times in order to obtain pure Fe<sub>3</sub>O<sub>4</sub> nanoparticles. Titania-coated  $\gamma$ -Fe<sub>2</sub>O<sub>3</sub> samples were prepared by the following method: tetra-*n*-butyl titanate (5 ml) was added to 25 ml of ethanol, and the resulting solution was stirred in an ice bath. To a second 25 ml portion of ethanol, 1 ml of water and 0.02 ml of HCl were added. The ethanol/water/HCl solution was slowly added to the tetra-*n*-butyl titanate/ethanol solution under stirring and cooling with ice [17]. When the resulting mixture turned to milky white (sol formation), the Fe<sub>3</sub>O<sub>4</sub> nanoparticles was dispersed in it. The dispersion was placed in a supersonic bath, stirred vigorously with a glass-stirring rod, and kept at 25 °C throughout the whole process. After sonification for 30 min, 1–2 ml water was dripped into the dispersion at a rate of 0.5 ml min<sup>-1</sup> until the gel was formed. The gel was placed for 12 h at the room temperature and then baked for 6 h under an infrared lamp. The granulated gel was placed in a tube furnace (in air), the temperature was ramped (100 °C h<sup>-1</sup>) to 500 °C. The gel was sintered at this temperature for 6 h. Then the temperature was ramped back down (50 °C h<sup>-1</sup>) to room temperature. The crystalline phase as well as the grain size was determined by X-ray diffraction (XRD) method, transmission electron microscope (TEM) and atomic force microscope (AFM), respectively. In photocatalytic experiments, an aqueous solution of acridine dye (30 ml, 2.74 × 10<sup>-5</sup> mol l<sup>-1</sup>, pH 6.40) containing TiO<sub>2</sub>/ $\gamma$ -Fe<sub>2</sub>O<sub>3</sub> nanoparticles was stirred overnight in the dark to permit the adsorption/desorption equilibrium among the photocatalyst, dye, the solubilized oxygen, and the atmospheric oxygen. A 450 W medium mercury lamp as a visible light source was positioned within a cylindrical Pyrex vessel; water was circulated through the cylindrical Pyrex

vessel to avoid lamp overheating. A light filter completely removing wavelengths below 450 nm was placed outside the Pyrex thimble to guarantee irradiation with visible light. A 100 W Hg lamp was used as a UV light source. Four same acridine dye reaction solutions (each of 30 ml) were used around the radiation source. The 3 ml aliquots were taken from solutions irradiated for different time and separated though a centrifugal precipitator (4000 rpm min<sup>-1</sup>) prior to analysis. Variations in the concentration of dyes in each degraded solution were monitored by UV-Vis spectroscopy (absorption at  $\lambda_{\max}$  = 492 nm for acridine dye).

## 3. Results and discussion

### 3.1. XRD analysis

Fig. 1 shows the XRD patterns of Fe<sub>3</sub>O<sub>4</sub> powders sintered at 200, 500, 700 and 900 °C for 5 h in air atmosphere. It has been revealed from the XRD patterns that Fe<sub>3</sub>O<sub>4</sub> particles were oxidized and the  $\gamma$ -Fe<sub>2</sub>O<sub>3</sub> phase was formed at 200 °C, maghemite was transformed into hematite at 700 °C. The main phases are pure maghemite at 200 and 500 °C, pure hematite at 700 and 900 °C, respectively. The X-ray photographs of TF (TiO<sub>2</sub>:Fe<sub>2</sub>O<sub>3</sub> = 1:1) samples (Fig. 3) show that the phases prepared at different sintering temperatures of the powder sample are maghemite, anatase–maghemite, anatase–rutile–hematite and rutile–hematite–pseudobrookite (Fe<sub>2</sub>TiO<sub>5</sub>). Compared with XRD spectra of TiO<sub>2</sub> prepared under similar condition and sintered at 500 and 700 °C (Fig. 2), the presence of iron in the TF sample did not catalyze the transformation of anatase to rutile as reported by Palmisano and co-workers [18,19] in the TiO<sub>2</sub>/Fe<sub>2</sub>O<sub>3</sub> mixed oxide powders. The XRD pattern at low sintering temperature (500 °C) shows very broad peaks of anatase and narrow diffraction lines of maghemite phases. These results indicate that the small crystal size of TiO<sub>2</sub> powders in the samples is combined tightly on the surface of the  $\gamma$ -Fe<sub>2</sub>O<sub>3</sub> core, forming a TiO<sub>2</sub> shell. As can be seen from the XRD patterns (Figs. 1 and 2), with the increasing of sintering temperature, the diffraction lines become very narrow and sharp which reveals a large particle size distribution of the crystal. As shown in Fig. 3, although the crystalline phase of Fe<sub>2</sub>O<sub>3</sub> changes with increasing sintering temperature, the breadth of Fe<sub>2</sub>O<sub>3</sub> particle diffraction lines has hardly any variety in the TF sample. The reason for this is that the TiO<sub>2</sub> shells on the surface of the  $\gamma$ -Fe<sub>2</sub>O<sub>3</sub> core prevented reunion between  $\gamma$ -Fe<sub>2</sub>O<sub>3</sub> particles sintered at high temperature. The TF sample sintered at 900 °C consists of a fraction of Fe<sub>2</sub>TiO<sub>5</sub> phase together with the rutile phase compared with the sample fired at low temperature, for there is little tendency of bulk reaction between  $\gamma$ -Fe<sub>2</sub>O<sub>3</sub> and TiO<sub>2</sub> particles at low temperature. But the sample prepared at higher temperature, irrespective of the preparative methods, TiO<sub>2</sub> was always found to be in the rutile phase. The formation of pseudobrookite phase can be explained by

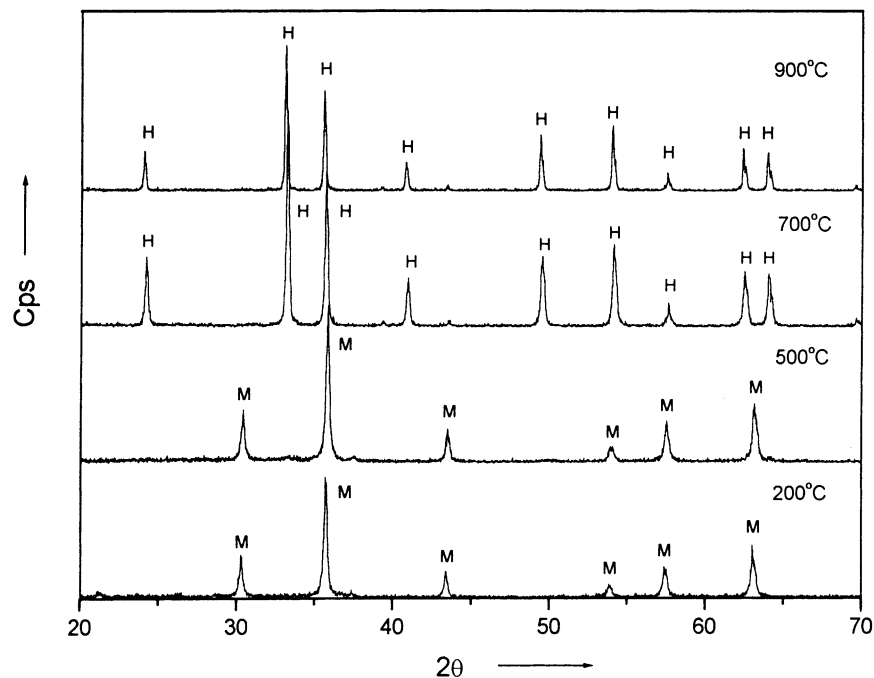


Fig. 1. XRD patterns of  $\text{Fe}_3\text{O}_4$  sintered at different temperatures. M: maghemite, H: hematite.

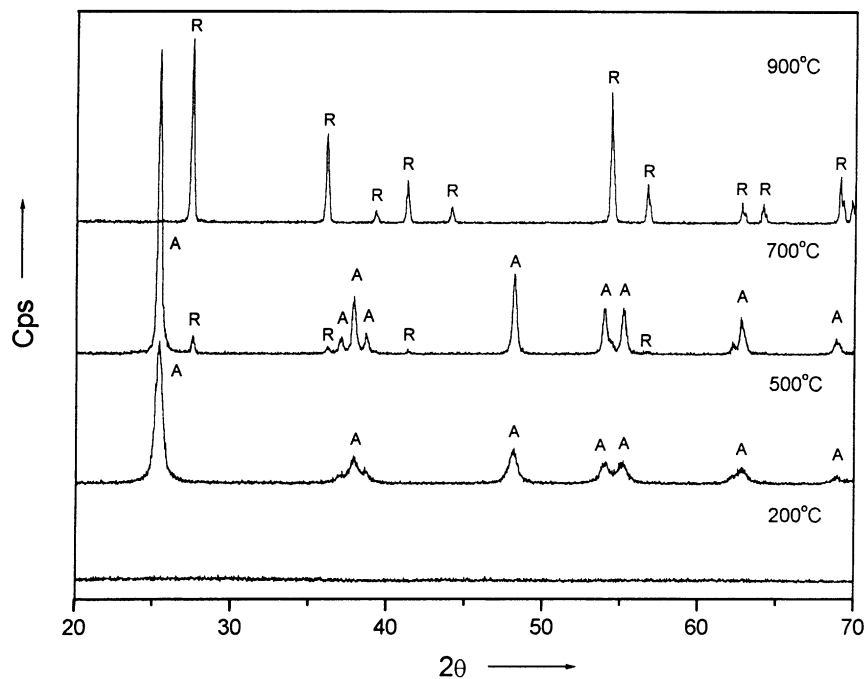


Fig. 2. XRD patterns of  $\text{TiO}_2$  sintered at different temperatures. A: anatase, R: rutile.

the fact that at higher temperature, certain percentage of the  $\text{Fe}^{3+}$  ions present at the surface of  $\gamma\text{-Fe}_2\text{O}_3$  core diffuses into the  $\text{TiO}_2$  shell producing a substitutional solid solution in which  $\text{Fe}^{3+}$  is dispersed in the lattice of  $\text{TiO}_2$ . In fact, as the  $\text{Fe}^{3+}$  radius is similar to that of  $\text{Ti}^{4+}$ , the substitution of iron in the matrix of  $\text{TiO}_2$  is a favorable process, being easier in rutile due to the open channels present in this

structure and then forming mixed oxides such as  $\text{Fe}_2\text{TiO}_5$  phase between the  $\gamma\text{-Fe}_2\text{O}_3$  core and the  $\text{TiO}_2$  shell [20,21].

### 3.2. AFM and TEM studies

In order to probe the interaction among the constituents in the loaded photocatalyst system, the photocatalysts were

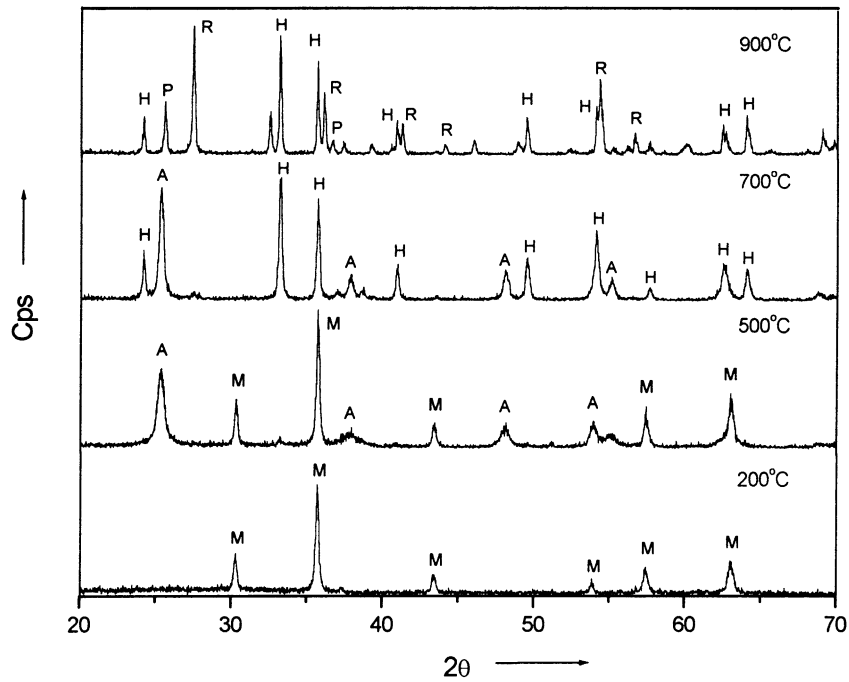


Fig. 3. XRD patterns of TF ( $\text{TiO}_2:\text{Fe}_2\text{O}_3 = 1:1$ ) sintered at different temperatures. A: anatase, R: rutile, M: maghemite, H: hematite, P: pseudobrookite.

investigated by AFM and TEM. The AFM photograph of the TF samples (Fig. 4) calcined at  $500^\circ\text{C}$  showed that various granular aggregates of  $\text{TiO}_2$  particles formed a shell enwrapping a core of  $\gamma\text{-Fe}_2\text{O}_3$  conglomeration tightly and regularly. This is further supported by TEM studies of the

samples sintered at 500 and  $900^\circ\text{C}$ , respectively. TEM photographs of F1 (a,  $\text{Fe}_2\text{O}_3$  calcined at  $500^\circ\text{C}$ ), F2 (b,  $\text{Fe}_2\text{O}_3$  calcined at  $900^\circ\text{C}$ ), TF1 (c,  $\text{TiO}_2:\text{Fe}_2\text{O}_3 = 1:1$  calcined at  $500^\circ\text{C}$ ), TF2 (d,  $\text{TiO}_2:\text{Fe}_2\text{O}_3 = 1:1$  calcined at  $900^\circ\text{C}$ ) are presented in Fig. 5. The  $\text{Fe}_2\text{O}_3$  particle size varies from

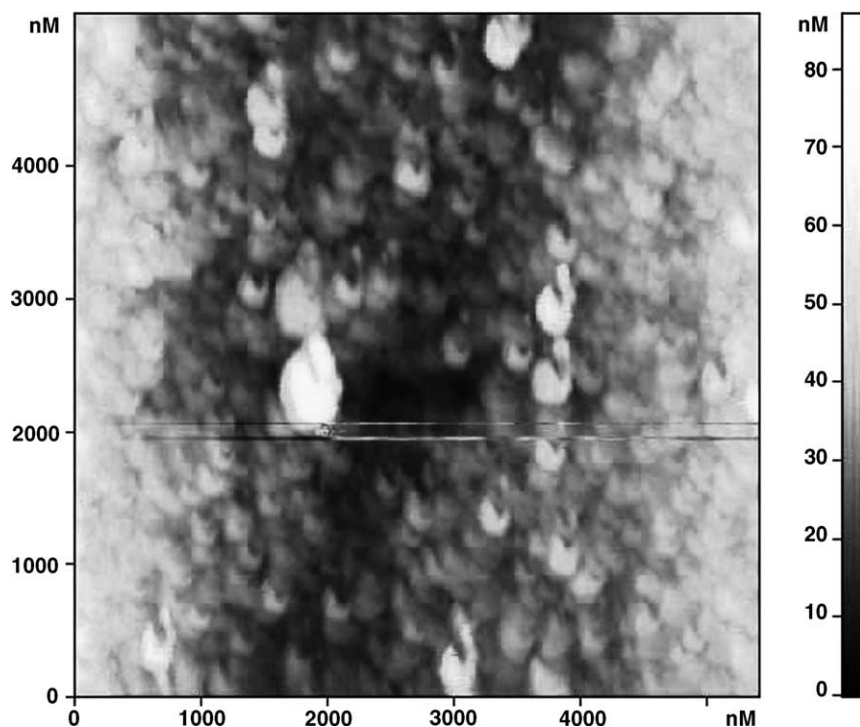


Fig. 4. AFM photograph of TF ( $\text{TiO}_2:\text{Fe}_2\text{O}_3 = 1:1$ ) samples sintered at  $500^\circ\text{C}$ .

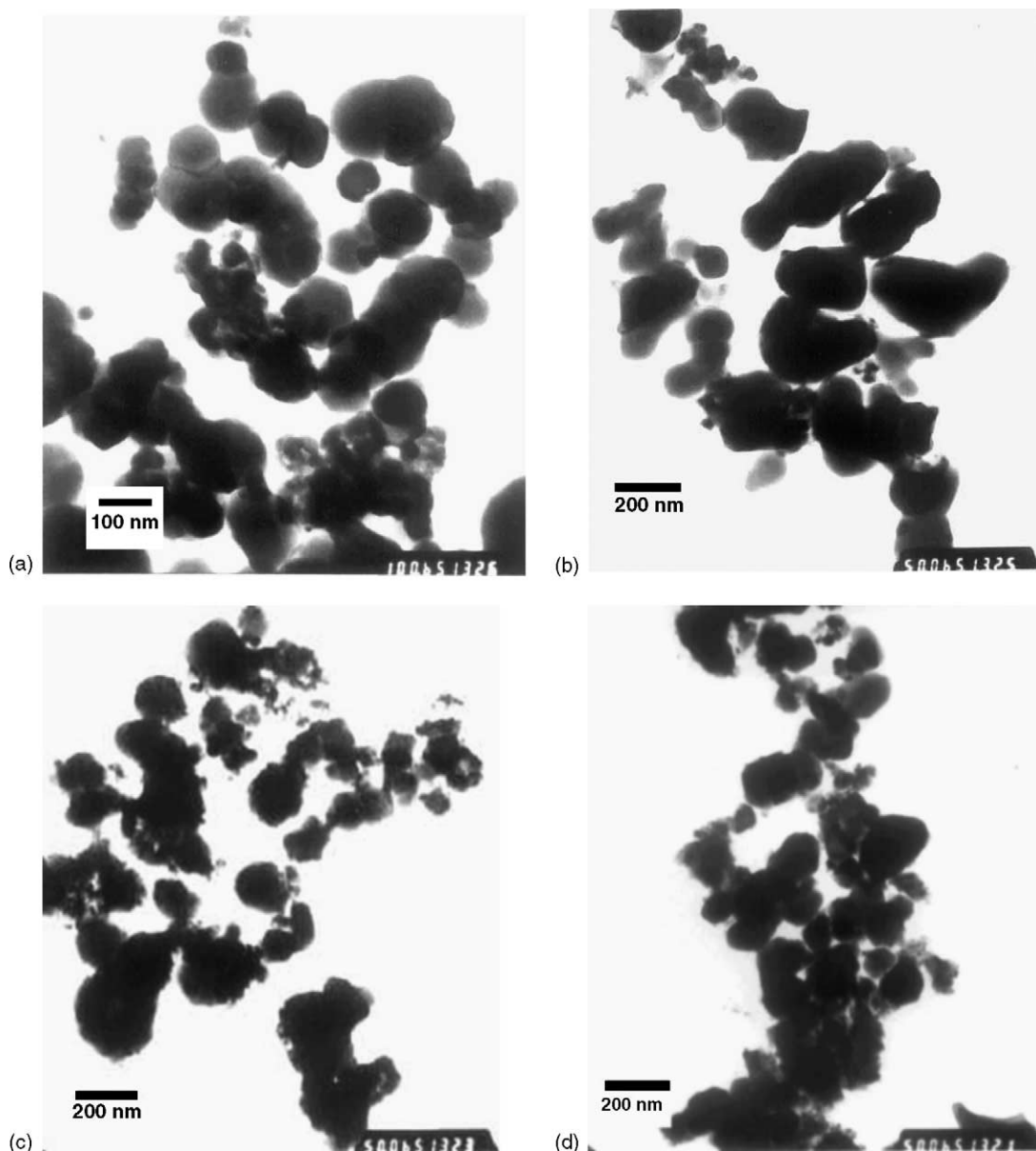


Fig. 5. TEM micrograph of samples: (a) F1:  $\text{Fe}_2\text{O}_3$  calcined at  $500^\circ\text{C}$ ; (b) F2:  $\text{Fe}_2\text{O}_3$  calcined at  $900^\circ\text{C}$ ; (c) TF1:  $\text{TiO}_2:\text{Fe}_2\text{O}_3 = 1:1$  calcined at  $500^\circ\text{C}$ ; (d) TF2:  $\text{TiO}_2:\text{Fe}_2\text{O}_3 = 1:1$  calcined at  $900^\circ\text{C}$ .

100 to 400 nm with increasing sintering temperature, as determined by TEM studies. This is in agreement with the XRD result where narrow and sharp peaks were appeared with increasing sintering temperature of the samples due to the increase of crystal size. But in the TF photocatalyst, comparing Fig. 5c and d with Fig. 5a and b, we found that the particle size has hardly any change with increasing sintering temperature. In addition, Fig. 5c and d shows that the particle size of  $\text{TiO}_2$  is also increased at  $900^\circ\text{C}$ , which is in agreement with XRD result, resulting in poor density of  $\text{TiO}_2$  membrane. Combining with the results of AFM measurements and the XRD patterns, it is shown that  $\text{Fe}_2\text{O}_3$  exists as a conglomeration with  $\text{TiO}_2$  very tightly combined on the surface of  $\text{Fe}_2\text{O}_3$  core as an

out-layer, forming a membrane preventing reunion between  $\gamma\text{-Fe}_2\text{O}_3$  particles at high temperature. It is clear that such a serried  $\text{TiO}_2$  membrane is favorable to restrain the adverse effect of  $\text{Fe}_2\text{O}_3$  particles on the  $\text{TiO}_2$  photocatalytic activity.

### 3.3. Photocatalytic activity

Photocatalyzed degradation of acridine dye under both UV and visible light irradiation was examined to reveal the effect of the  $\gamma\text{-Fe}_2\text{O}_3$  particle on the photocatalytic properties of titania. Titania was regarded as the only active material of these photocatalyst for photocatalysis and its dosage was constant in our experiments (15 mg titania in 30 ml

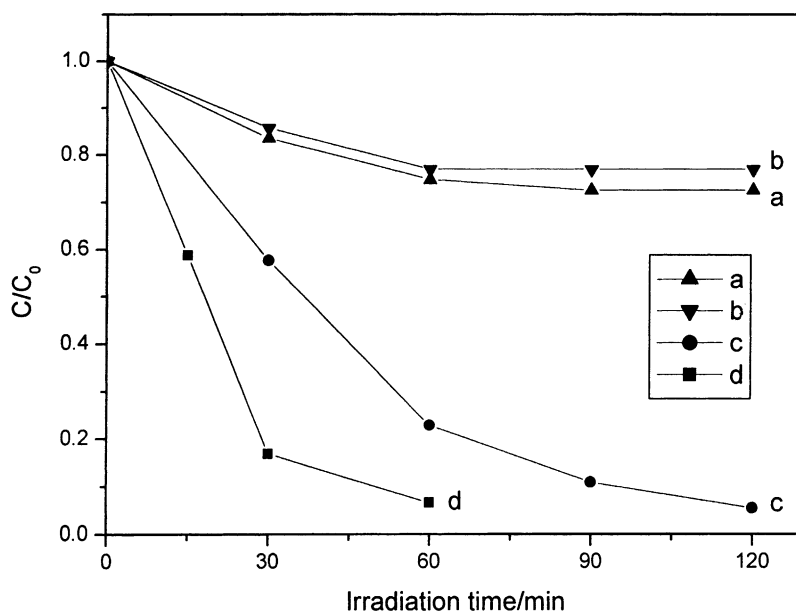


Fig. 6. Degradation of acridine dye ( $2.74 \times 10^{-5} \text{ mol l}^{-1}$ ) with different photocatalysts under UV irradiation: (a) blank; (b) F ( $0.5 \text{ g l}^{-1}$ ); (c) TF ( $1 \text{ g l}^{-1}$ ); (d)  $\text{TiO}_2$  ( $0.5 \text{ g l}^{-1}$ ).

solution) for an easy comparison of all the photocatalyst:  $0.5 \text{ g l}^{-1}$  T (pure  $\text{TiO}_2$ ) and  $1 \text{ g l}^{-1}$  TF ( $\text{TiO}_2:\gamma\text{-Fe}_2\text{O}_3 = 1:1$  calcined at  $500^\circ\text{C}$ ) in the experiment, respectively. Photodegradation result of acridine dye under UV irradiation is presented in Fig. 6. Curve (a) shows blank reaction, indicating that the dye degraded scarcely in the absence of photocatalyst and curve (b) shows that  $\gamma\text{-Fe}_2\text{O}_3$  has little photocatalytic activity under UV irradiation. In the experiments of curves (c) and (d), the same amount of titania

was used. Comparing with pure  $\text{TiO}_2$ , the photocatalytic of TF is not significantly depressed. Photodegradation rates of acridine dye under visible light irradiation are illustrated in Fig. 7. Different from the degradation under UV irradiation, the degradation of acridine dye with the photocatalyst TF under visible irradiation become slowly. However, the decoloration rate of acridine dye in the blank reaction is much faster than that under UV irradiation because of its self-photosensitization.

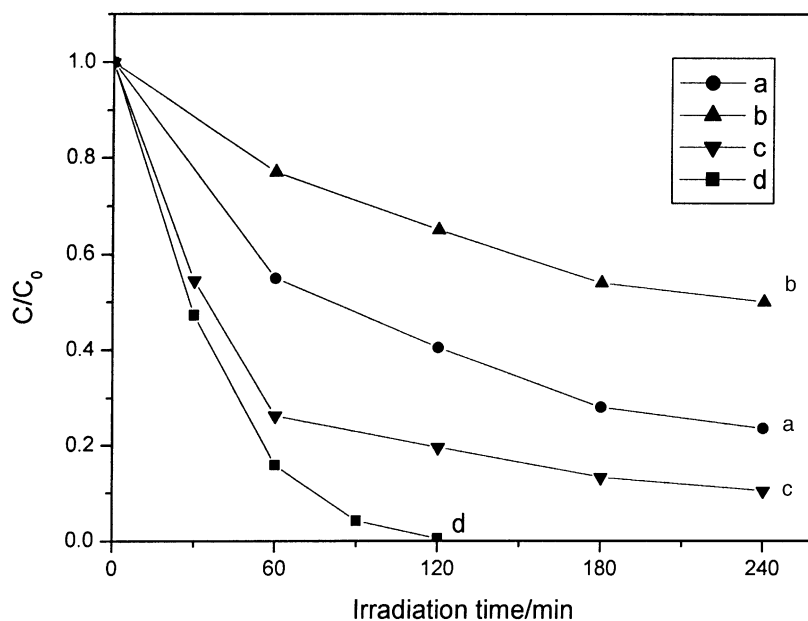


Fig. 7. Degradation of acridine dye ( $2.74 \times 10^{-5} \text{ mol l}^{-1}$ ) with different photocatalysts under visible light irradiation: (a) blank; (b) F ( $0.5 \text{ g l}^{-1}$ ); (c) TF ( $1 \text{ g l}^{-1}$ ); (d)  $\text{TiO}_2$  ( $0.5 \text{ g l}^{-1}$ ).

The adverse influence of the  $\gamma$ -Fe<sub>2</sub>O<sub>3</sub> under visible irradiation is similar to that under UV irradiation. Strong light absorption of the  $\gamma$ -Fe<sub>2</sub>O<sub>3</sub> cores under either UV or visible irradiation is one of the important reasons for the lower photocatalytic activity of the loaded catalyst. Because of the strong absorption of the  $\gamma$ -Fe<sub>2</sub>O<sub>3</sub> cores, the self-photosensitization of the dye is markedly weakened, and the decoloration of the dye under visible irradiation with F (Fig. 7b) is much slower than that in the blank reaction (Fig. 7a). Another important reason is related to the photocatalytic mechanism by UV and visible irradiation. The photocatalytic mechanism under visible irradiation is believed to involve electron transfer from an excited state of acridine dye to photocatalyst particles [22–24]. The excited dyes inject electrons to the conduction band (CB) of the titania, then the injected electrons react with the preadsorbed oxygen to form oxidizing species (O<sub>2</sub><sup>•-</sup>, <sup>•</sup>OOH, and then <sup>•</sup>OH radicals) that can bring about the photooxidation of dyes [2,25,26]. After well-knitting of the titania nanoparticles with the  $\gamma$ -Fe<sub>2</sub>O<sub>3</sub> cores (photocatalyst TF), a competitive process happens in which the generated CB electrons not only react with the oxygen but also inject into the conduction of the  $\gamma$ -Fe<sub>2</sub>O<sub>3</sub>, because the CB energy of  $\gamma$ -Fe<sub>2</sub>O<sub>3</sub> is lower than that of titania ( $E_{CB}(\text{TiO}_2) = -0.5 \text{ V vs. NHE at pH 7}$ ,  $E_{CB}(\gamma\text{-Fe}_2\text{O}_3) = 0.1 \text{ V vs. NHE at pH 7}$ ). Because of little activity of  $\gamma$ -Fe<sub>2</sub>O<sub>3</sub>, the photocatalytic activity of TiO<sub>2</sub>/ $\gamma$ -Fe<sub>2</sub>O<sub>3</sub> is depressed. Under UV illumination, titania absorbs photons with energy larger than the band gap of the titania to produce electron–hole couples. The produced CB electrons can also inject rapidly into the CB of the  $\gamma$ -Fe<sub>2</sub>O<sub>3</sub> cores; and the produced valence band (VB) holes not only inject into the VB of the  $\gamma$ -Fe<sub>2</sub>O<sub>3</sub> cores since the VB energy of the  $\gamma$ -Fe<sub>2</sub>O<sub>3</sub> is higher than that of the titania

( $E_{CB}(\text{TiO}_2) = 2.7 \text{ V vs. NHE at pH 7}$ ,  $E_{CB}(\gamma\text{-Fe}_2\text{O}_3) = 2.3 \text{ V vs. NHE at pH 7}$ ), but also cause photocatalytic reaction of the substrate. As a good electron–hole recombination center,  $\gamma$ -Fe<sub>2</sub>O<sub>3</sub>, which has little photocatalytic activity (as shown by curve (b) in Fig. 6), greatly depressed the photocatalytic activity of the loaded photocatalyst.

The effect of photocatalytic activity of TF samples fired at different temperature on the rate of destruction of acridine dye is shown in Fig. 8. The photocatalytic decolorization of acridine dye is a pseudo-first-order reaction and its kinetics may be expressed as follows:

$$\ln\left(\frac{C_0}{C}\right) = kt \quad (1)$$

where  $k$  is the apparent reaction rate constant,  $C_0$  and  $C$  are the initial concentration and the reaction concentration of acridine dye, respectively. It can be observed that the plot of  $\ln(C_0/C)$  vs. irradiation time for degradation of acridine dye is rapidly diminishing with increasing calcination temperature of the TF samples. The degradation rate decreases with the sintering temperature due to the presence of different crystalline phases (anatase and rutile) at various temperatures as observed in XRD analysis. There are two main reasons that influence the catalytic activity of the TF samples and lead to the results of Fig. 8. One is the change of particle size with the increasing sintering temperature of the specimens. Although the fine titania particles on the Fe<sub>2</sub>O<sub>3</sub> surface prevent conglomeration between Fe<sub>2</sub>O<sub>3</sub> particles and the particle size of Fe<sub>2</sub>O<sub>3</sub> core does not change significantly, the out-layer of TiO<sub>2</sub> particles reveals a large particle size distribution with the high firing temperature. Another reason can be attributed to the variation of phase composition. Due to the gradual development of rutile phase along with

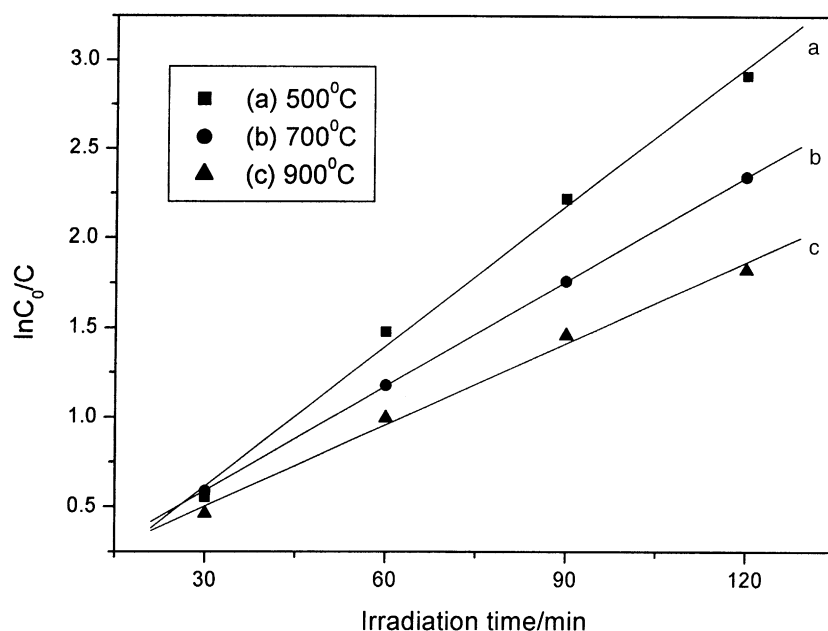


Fig. 8. Effect of photocatalytic activity of TF samples sintered at various temperatures: (a) 500 °C; (b) 700 °C; (c) 900 °C.

the  $\text{Fe}^{3+}$  ions dispersed in the lattice of  $\text{TiO}_2$  becoming the  $\text{Fe}_2\text{TiO}_5$  phase at higher firing temperatures ( $900^\circ\text{C}$ ), the catalytic activity reduces to a great extent.

To evaluate the influence of the amount of titania on the photocatalytic performance of magnetically separated photocatalyst, three samples were prepared at  $500^\circ\text{C}$ : TFa ( $\text{TiO}_2:\gamma\text{-Fe}_2\text{O}_3 = 3:7$ ), TFb ( $\text{TiO}_2:\gamma\text{-Fe}_2\text{O}_3 = 1:1$ ) and TFc ( $\text{TiO}_2:\gamma\text{-Fe}_2\text{O}_3 = 7:3$ ) containing 30, 50 and 70% of  $\text{TiO}_2$  nanoparticles, respectively. The result shows that the degradation rate increased with the increasing amount of supported  $\text{TiO}_2$  in an apropos concentration range of acridine dye ( $k_{\text{TFa}} = 5.47 \times 10^{-3} \text{ min}^{-1}$ ,  $k_{\text{TFb}} = 2.61 \times 10^{-2} \text{ min}^{-1}$ ,  $k_{\text{TFc}} = 2.65 \times 10^{-2} \text{ min}^{-1}$ ). After being used three times, the degradation rate of TFa and TFb is hardly any depressed, but the degradation rate of TFc decreases by 30% (for tests 1, 2 and 3, the rate constants are  $2.65 \times 10^{-2}$ ,  $2.11 \times 10^{-2}$  and  $1.54 \times 10^{-2} \text{ min}^{-1}$ , respectively). This decreasing activity is probably due to a small part of  $\text{TiO}_2$  particles that takes off from the  $\gamma\text{-Fe}_2\text{O}_3$  core and is eliminated after the first step. Consequently, the  $\text{TiO}_2$  concentration is lower than  $0.5 \text{ g l}^{-1}$ . On the other hand, when the amount of  $\text{TiO}_2$  was 30% in the TF samples like TFa, the surface of  $\gamma\text{-Fe}_2\text{O}_3$  core was not fully coated by  $\text{TiO}_2$  nanoparticles. Strong light absorption of the  $\gamma\text{-Fe}_2\text{O}_3$  cores under light irradiation causes the lower photocatalytic activity of TFa sample. Therefore, the optimal supporting amount of  $\text{TiO}_2$  is about 50%.

## Acknowledgements

This study was supported by Natural Science Foundation of China (QT program).

## References

- [1] R.W. Matthews, *Water Res.* 24 (1990) 653.
- [2] M.R. Hoffmann, S.T. Martin, W. Choi, D.W. Bhemann, *Chem. Rev.* 95 (1995) 69.
- [3] A. Fujishima, T.N. Rao, D.A. Tryk, *J. Photochem. Photobiol. C* 1 (2000) 1.
- [4] J.M. Herrmann, *Catal. Today* 53 (1999) 115.
- [5] R.W. Mathews, *J. Catal.* 111 (1988) 264.
- [6] N. Negishi, T. Iyoda, K. Hashimoto, A. Fujishima, *Chem. Lett.* (1995) 841.
- [7] M.A. Fox, M.T. Dulay, *Chem. Rev.* 93 (1993) 341.
- [8] A.P. Davis, D.L. Green, *Environ. Sci. Technol.* 33 (1999) 609.
- [9] J. Fernandez, J. Bandara, A. Lopez, P. Albers, J. Kiwi, *Chem. Commun.* (1998) 1493.
- [10] D. Robert, A. Piscopo, O. Heintz, J.V. Weber, *Catal. Today* 54 (1999) 291.
- [11] Y.H. Hsien, C.F. Chang, Y.H. Chen, S. Cheng, *Appl. Catal. B* 31 (2001) 241.
- [12] Y. Ma, J.B. Qiu, Y.A. Cao, Z.S. Guan, J.N. Yao, *Chemosphere* 44 (2001) 1087.
- [13] V. Stafford, K.A. Gray, P.V. Kamat, *J. Phys. Chem.* 98 (1994) 6343.
- [14] A. Modestov, V. Glezer, I. Marjasin, O. Lev, *J. Phys. Chem. B* 101 (1997) 4623.
- [15] F. Chen, J. Zhao, *Catal. Lett.* 58 (1999) 245.
- [16] L.W. Chen, P.P. Zhang, J.S. Jiang, N.F. Zhou, *Acta Phys.-Chim. Sin.* 6 (1990) 88.
- [17] B.B. Lakshmmi, P.K. Dorhout, C.R. Martin, *Chem. Mater.* 9 (1997) 857.
- [18] J.A. Navío, M. Macías, M. González-Catalán, A. Justo, *J. Mater. Sci.* 27 (1992) 3036.
- [19] R.I. Bickley, T. González-Carreño, L. Palmisano, *Mater. Chem. Phys.* 29 (1991) 475.
- [20] A. Amorelli, J.C. Evans, C.C. Rowlands, *J. Chem. Soc., Faraday Trans. I* 85 (1989) 4031.
- [21] D. Gazzoli, G. Minelli, M. Valigi, *Mater. Chem. Phys.* 21 (1989) 93.
- [22] J. Zhao, T. Wu, K. Wu, K. Oikawa, H. Hidaka, N. Serpone, *Environ. Sci. Technol.* 32 (1998) 2394.
- [23] L. Zang, P. Qu, J. Zhao, T. Shen, H. Hidaka, *Chem. Lett.* (1997) 791.
- [24] J. He, J. Zhao, T. Shen, H. Hidaka, N. Serpone, *J. Phys. Chem. B* 101 (1997) 9027.
- [25] P.V. Kamat, S. Das, K.G. Thomas, M.V. George, *Chem. Phys. Lett.* 178 (1991) 75.
- [26] F. Willing, R. Eichberger, N.S. Sunsaesan, B.A. Parkinson, *J. Am. Chem. Soc.* 112 (1990) 2702.